DISSECTING THE POLYHYDROXYALKANOATE-BINDING DOMAIN OF THE PhaF PHASIN: RATIONAL DESIGN OF A MINIMIZED AFFINITY TAG

Running title: Rational design of a minimized PHA affinity tag

Aranzazu Mato[a,b,†], Francisco G. Blanco[a,b,†], Beatriz Maestro[c], Jesús M. Sanz[c,d], Jesús Pérez-Gil[e] and M. Auxiliadora Prieto[a,b*]

[a]Polymer Biotechnology Group. Microbial and Plant Biotechnology Department, Centro de Investigaciones Biológicas Margarita Salas-CSIC, Madrid, Spain.

[b]Interdisciplinary Platform for Sustainable Plastics towards a Circular Economy-Spanish National Research Council (SusPlast-CSIC), Spain.

[c]Host-parasite Interplay In Pneumococcal Infection Group. Microbial and Plant Biotechnology Department, Centro de Investigaciones Biológicas Margarita Salas-CSIC, Madrid, Spain.

[d]Centro de Investigación Biomédica en Red de Enfermedades Respiratorias (CIBERES), Madrid, Spain

[e]Biochemical and Molecular Biology Department, Facultad de Ciencias Biológicas, Universidad Complutense de Madrid, Madrid, Spain.

[†]These authors contributed equally to this work. Order was decided by seniority.

* Corresponding Author. mailto:auxi@cib.csic.es

ABSTRACT

Phasin PhaF from *Pseudomonas putida* consists of a modular protein whose N-terminal domain (BioF) has been demonstrated to be responsible for the binding to the PHA granule. BioF has been exploited with biotechnological purposes as an affinity tag in the functionalization of PHA beads with fusion proteins both *in vivo* and *in vitro*. The structural model of this domain suggests an amphipathic α-helical conformation with the hydrophobic residues facing the PHA granule. In this work, we have analyzed the mean hydrophobicity and the hydrophobic moment of the native BioF tag to rationally design shorter versions that maintain the affinity for the granule. Hybrid proteins containing the green fluorescent protein (GFP) fused to the BioF derivatives were studied for *in vivo* localization on the PHA, stability on the surface of the PHA granule against pH, temperature and ionic strength, and their possible influence on the PHA synthesis. Based on the results obtained, a minimized BioF tag for PHA functionalization has been proposed (MinP), which retains similar binding properties but possesses an attractive biotechnological potential derived from its reduced size. The MinP tag was further validated by analyzing functionality and stability of the fusion proteins MinP-β-galactosidase and MinP-CueO from *Escherichia coli*.

IMPORTANCE

Polyhydroxyalkanoates (PHAs) are biocompatible, non-toxic and biodegradable biopolymers with exceptional applications in the industrial and medical fields. The complex structure of the PHA granule can be exploited as a toolbox to display molecules of interest on their surface. Phasins, the most abundant group of proteins on the granule, have been employed as anchoring tags to obtain functionalized PHA beads for high-affinity bioseparation, enzyme immobilization, diagnostics or cell targeting. Here, a shorter module

based on the previously designed BioF tag has been demonstrated to maintain the affinity for the PHA granule, with higher stability and similar functionalization efficiency. The use of a 67 % shorter peptide, which maintains the binding properties of the entire protein, constitutes an advantage for the immobilization of recombinant proteins on the PHA surface both *in vitro* and *in vivo*.

INTRODUCTION

Display of functional proteins on solid supports constitutes an important tool for many industrial and biomedical purposes (1). In this vein, nanoparticles functionalized with peptides and proteins may be widely employed for therapeutic applications, acting as drug carriers, anti-tumor and bactericidal drugs or cellular targeting moieties (2). Strategies for protein immobilization vary depending on the matrixes employed and the final application, and they may include non-specific adsorption, chemical cross-linking or the use of affinity tags (3).

The biodegradable and biocompatible polyhydroxyalkanoates (PHA) are bacterial storage polyesters which are gaining much attention as highly-tunable materials for the development of a variety of biomedical and industrial devices. This is mainly due to the structural versatility that can be obtained by bacterial fermentation and post-biosynthetic modifications (4). These polymers are synthetized as hydrophobic inclusions surrounded by a layer of proteins involved in the PHA metabolism, called granule associated proteins (GAPs). Among them, the most remarkable are PHA polymerases and depolymerases, as well as phasins, which are amphipathic proteins coating the PHA granule (Fig. 1) (5). The complex architecture of PHA granules offers a toolbox to display molecules of interest on their surface (6). GAPs have been used as anchoring tags to immobilize value-added proteins on the surface of PHA materials. Depending on the target application, functionalization by using GAP-fusion proteins may be achieved *in vivo* (simultaneously to the PHA production in the bacterial cytoplasm) or *in vitro* (utilizing endotoxin free PHA purified after the biotechnological production) (7). The first strategy led to GAP-fusion proteins immobilized onto the PHA surface

73 simultaneously with their synthesis. The second approach requires the extraction of the
74 polyester, its conversion into nanoparticles or films, and the subsequent *in vitro*
75 immobilization of the GAP-fusion. This strategy is convenient for biomedical purposes
76 that require endotoxin-free PHA materials and a control of the amount of the immobilized
77 protein. Among GAPs, phasins constitute the most abundant group of proteins covering
78 the granule (8, 9) and have been widely used as anchoring tags to functionalize PHA
79 supports for a variety of applications such as affinity bio-separation (10), protein
80 purification (11-13), enzyme immobilization (14-16), protein delivery to natural
81 environments (17), diagnostics (18, 19), cell targeting (20-24) and antimicrobials (25).

82 PhaF from *Pseudomonas putida* is a prototypic and well characterized phasin (26, 27).
83 It is a partially intrinsically disordered protein consisting of two domains connected by a
84 leucine zipper motif that is responsible for its oligomerization (28, 29). The 142-aa
85 BioF module, containing the N-terminal and the leucine zipper sequences, has been
86 extensively demonstrated to bind to PHA granules (17, 30, 31). Even more, the BioF
87 domain binds not only to PHA materials *in vitro* but also to other hydrophobic-
88 hydrophilic interfaces such as those containing phospholipids, making it a versatile tag
89 to combine with a variety of hydrophobic supports (14, 32). One of the drawbacks of
90 applying the BioF tag for biomedical applications is its size, as a smaller peptide would
91 be more desirable to reduce potential interferences with correct folding and activity of
92 the tagged protein of interest (33).

93 Based on the predicted structural model of PhaF that supports a conformation-dependent
94 binding of the BioF fragment to the PHA granule (28), we have explored the ability of
95 reduced segments of BioF to maintain the capacity to bind PHA, with the aim of finding

a shorter, yet fully functional, BioF segment to be used as an efficient affinity tag for recombinant protein immobilization.

RESULTS

BioF-based-tag design based on structure prediction

The N-terminal domain of the PhaF (N-PhaF) is predicted to form a long, largely amphipathic α-helix that interacts with PHA through hydrophobic interactions while exposing the hydrophilic side to solvent or cytoplasmic fraction of the cell (27). A *HeliQuest* analysis of the N-PhaF sequence shows the mean hydrophobicity (⟨*H*⟩) and the amphipaticity (*i.e.*, hydrophobic moment, ⟨μ*H*⟩) of all possible 18-aa α-helical stretches within this domain (Fig. 2A) and reveals fluctuations of both properties throughout the domain. Interestingly, the region consisting of residues 33-49 simultaneously exhibits relatively high values of both ⟨*H*⟩ and ⟨μ*H*⟩, while residues 58-91 displayed the lowest values of ⟨*H*⟩ and ⟨μ*H*⟩. This latter region has been suggested to be natively unfolded in solution when not complexed with PHA (28) (Fig. 2A). To further determine the contributions of different segments of N-PhaF to the binding to PHA, we designed shortened versions of BioF (Fig. 2B), differing in polarity, amphipaticity and length, namely Bi1, Bi2, Bi3 and Bi4. The Bi1 segment contains the N-terminal region and the most hydrophobic stretches, including the 26-32 subsequence (WLAGLGI) that is conserved in all PhaF-like phasin proteins and has been proposed to play a fundamental role in the interaction of phasins with PHA granules (30). Bi2 contains the 33-49 subsequence mentioned above, whereas Bi3 starts with the Bi2 segment and extends to contain the central leucine zipper region. Finally, the Bi4 segment was designed on a different basis, as it only contains the predicted leucine zipper motif involved in PhaF oligomerization along with a short adjacent sequence (28, 29).

In vivo localization of BioF-based fragments in P. putida KT2440

120 To study the *in vivo* PHA binding properties of the different Bi segments, we designed
121 several green fluorescent protein (GFP) fusion constructs, which allowed for the determination
122 of their intracellular localization. Each construct (named Bi1-G, Bi2-G, Bi3-G, Bi4-G and
123 BioF-G) was inserted in the pSEVA238 plasmid under the control of the XylS/P*m*
124 regulator/promoter system (Table 3) (35) and introduced into *P. putida* KT2440. Cultures
125 were grown in 0.1 N M63 plus 15 mM of octanoate to favour PHA accumulation, and the
126 productionof the corresponding recombinant protein was induced at $O.D._{600}$ 0.8 by the addition
127 of 1 mM of 3-methylbenzoate (3-MB). After 24 h of growth, cells were observed through
128 epifluorescence microscopy (Fig. 3A). A common phenotype was detected in the strains
129 containing BioF-G, Bi1-G, Bi3-G, and Bi4-G fusions, which showed an enriched ring of
130 fluorescence surrounding the PHA granules (Fig. 3A). This pattern suggests the localization
131 of these fusion proteins on the surface of the granules. A different phenotype could be observed
132 in cells containing the shortest segment Bi2-G, in which the protein was observed to be
133 homogeneously distributed throughout the cytoplasm. This localization technique was
134 complemented by glycerol gradient separation and isolation of PHA granules from cells
135 producing the Bi-G segments (see Materials and Methods section for details). Supernatant and
136 pellet fractions of crude extracts and purified granules were separated by SDS-PAGE (Fig.
137 3B). Bi1-G, Bi3-G and BioF-G proteins were detected in the granule fraction while Bi2-G was
138 only detected in the supernatant of the crude extract, validating the results obtained
139 microscopically. Some Bi3-G and BioF-G proteins were also detected in the supernatant fraction
140 of the crude extract. The inability to detect Bi4-G in any fraction by SDS-PAGE suggests either
141 that this polypeptide is produced at a low level, it is unstable, or forms aggregates that cannot
142 enter the gel. Due to these possibilities the Bi4 segment was discarded for further studies.

In vivo localization of BioF-based fragments in a P. putida KT2440 Δpha strain containing PhaC1 synthase

Phasins covering the PHA granule have been demonstrated to interact with other granule associated proteins (GAPs) through the leucine zipper motif (29). In order to avoid potential interference by the presence of other GAPs on the surface of the PHA granule, a *P. putida* KT2440 mutant lacking the *pha* gene cluster was employed as a host to introduce solely the *phaC1* synthase gene, sufficient to produce a low level of PHA. The *phaC1* expression was under the control of a weak constitutive promoter and integrated in the chromosome via the pTn*7*-M transposon system. The resulting strain was named Δ*pha+C1* and employed to confirm the ability of the Bi fragments to maintain their affinity for the PHA granule in the absence of other phasins and GAP proteins.

The plasmids coding the different Bi segment-GFP fusion constructs were introduced into the Δ*pha+C1* strain and assessed for localization by epifluorescence microscopy. The Bi1-G protein was observed to localize in rings surrounding the PHA granules as the control BioF-G protein (Fig. 4A), and both proteins were detected in the pellet and PHA granule fractions, with additional presence of BioF-G in the supernatant portion (Fig. 4B). Bi3-G showed a similar localization pattern as BioF-G, with some fluorescence observed in the cytoplasm out from the granule surface (Fig. 4A). These results are in agreement with the fractionation studies (Fig. 4B), as some Bi3-G and BioF-G were detected in the soluble fraction. Besides, some degradation of Bi3-G seemed to occur indicated as double red arrows in Fig. 4B. In the case of Bi2-G, the fluorescence was found distributed inside the whole cell suggesting again that this segment is unable to bind to PHA granules (Fig. 4A). This hypothesis is further

165 confirmed by the lack of granule association in the fractionation experiment (Fig. 4B).

166 ***Stability of BioF-based structures on the PHA granule***

167 Previous work had demonstrated the stability of adsorption of BioF fusion proteins to isolated
168 PHA granules through the application of a panel of detergents (14, 30). One of the most effective
169 detergents for disrupting the BioF-PHA granule interaction is Triton X-100. Thus, we used this
170 detergent to assess the binding strength of the three efficient adsorption variants to PHA, Bi1-
171 G, Bi3-G and BioF-G. PHA granules isolated from a 50 mL culture of *P. putida* KT2440
172 Δ*pha+C1* strains were resuspended in different concentrations of Triton X-100 and incubated 2
173 h at room temperature. After the treatment, the supernatant and pellet fractions of the suspension
174 were separated, and the protein released from the granules was evaluated by SDS-PAGE (Fig.
175 S1).

176 The gel band intensities were used to calculate the percentage of Bi segment protein released
177 from the PHA granules (Fig. 5). The data indicates that Bi3-G presents the weakest interaction
178 with the PHA granules, even in the absence of detergent. In contrast, the protein Bi1-G was not
179 released in the absence of detergent and, in any case, it remained adsorbed in ca. 90 % on the
180 granule even at 1.5 % of Triton X-100, surpassing the native BioF-G. This indicates that Bi1
181 displays an affinity to PHA granules similar or even higher than BioF and therefore we
182 focused our efforts to further evaluate this segment as a potential tag for biotechnological uses.

183 Next, the stability of the binding between Bi1-G and PHA granules under different
184 physicochemical conditions (temperature, ionic strength and pH) was evaluated. An aliquot of
185 PHA granules containing Bi1-G was resuspended in buffer containing the specified condition

186 and incubated for 2 h at the indicated temperature, or otherwise 4 °C, and followed by separation
187 of the supernatant and pellet fractions. As can be observed in Fig. 6, the protein mostly remained
188 attached to the granule at the different temperatures (-20 °C, 4°C, 37 °C and 60 °C), ionic
189 strengths (10 mM, 100 mM and 1 M NaCl) and pH's (pH 3.0, pH 5.0, pH 7.0 and pH 9.0)
190 tested, although some degradation occurred upon incubation at pH 3.0.

191 ***Influence of fusion proteins on PHA production and functionalization efficiency***

192 The Bi1 segment was considered a promising choice as an optimized PHA affinity tag due to
193 the short size of the fragment, co-localization with PHA granules *in vivo* and its persistent
194 interaction with PHA *ex vivo* under different physicochemical conditions, comparable to the
195 BioF-PHA interaction. With the aim of studying the potential of Bi1 to be used as an affinity
196 tag, the effect of the production of this protein on PHA production and PHA granule
197 functionalization was evaluated. Strains producing BioF-G and Bi1-G, or harbouring an empty
198 vector as a control, were analysed for PHA production (Table 1). The presence of any plasmid
199 whether empty vector or BioF-G or Bi1-G encoding genes resulted in a roughly 20 % decrease
200 in PHA production in recombinant strains. Interestingly, in the *Δpha+C1* background the
201 presence of the whole BioF increased the percentage of PHA when compared to Bi1-G producing
202 or empty vector cells, 38 % versus ~27 %, respectively. Conversely, this effect was not
203 maintained in the wild type strain, where the PHA accumulation was similar among all the
204 strains containing plasmid. The concentration of granule-associated proteins was also measured
205 by quantifying bands from SDS-PAGE isolated PHA granules. In the Δ*pha+C1* background, a
206 higher amount of granule-associated BioF-G (8 mg per gram of PHA) was observed compared
207 to Bi1-G (5.8 mg per gram of PHA). However, in molar terms, little difference was detected

between the two segments, with the presence of protein at 0.17 μM and 0.16 μM per gram of PHA for BioF-G and Bi1-G, respectively.

Construction of a plasmid based on Bi1 for PHA functionalization

The Bi1 fragment demonstrated an interaction with PHA granules with superior functionalization efficiency and a strong stability making this construct suitable to be used as a tag to display functional proteins on the surface of PHA materials. Based on this optimized tag, hereafter named MinP, a fusion plasmid based on pSEVA238 was designed to simplify the production of protein-functionalized PHA nanobeads. The MinP fusion plasmid allows for induced expression under the control of *xylS*/P_m system and was modified to incorporate a RBS followed by the MinP tag in order to allow N-terminal fusions of the protein of interest (Fig. 7A). The novel plasmid, called pSMinPN, contains a multicloning site (MCS) separated from the *minP* sequence by a glycine-rich linker region (*Linker*) which can be removed if desired by using two engineered flanking *Xho*I sites. This linker can also be replaced by other spacer regions or to include an intein site, expanding its potential applications. As a proof of concept, a *minP-GFP* fusion gene was constructed in pSMinPN, transformed into *Δpha+C1*, and co-localization of MinP-GFP with PHA granules was observed by florescence microscopy following induction (Fig. 7B).

Validation of the MinP tag for enzymes immobilization

To validate the MinP as affinity tag, two enzymes, the β-galactosidase and the CueO oxidase from *E. coli* were genetically fused to *minP* by using the designed plasmid pSMinPN. Both enzymes are of wide applicability in the food industry for manufacturing lactose-hydrolyzed

products and production of galactosylated products, in the case of the β-galactosidase (36), and for the textile and paper industries as well as for organic compounds degradation with CueO oxidase (15, 37). The β-galactosidase coding gene was introduced by conventional cloning into *Xho*I and *Bam*HI sites, resulting in pSMinP-2 plasmid, and the c*ueO* gene into *Xho*I and *Hind*III sites resulting in the plasmid pSMinP-3. Both were independently transferred to *P. putida* KT2440 Δ*pha*+C1 and both strains, KT2440 Δ*pha*+C1 (pSMinP-2) and *P. putida* KT2440 Δ*pha*+C1 (pSMinP-3) were able to produce the fusion proteins of 122 kDa and 59 kDa respectively (Fig S2). The fusion proteins were able to bind to the PHA granules, and the binding stability under different physicochemical conditions (temperature, ionic strength and pH) was evaluated as described above. As can be observed in Table 2, the fusion proteins remained attached to the granules at percentages ≥ 85 % in all conditions for both MinP-β-galactosidase and MinP-CueO (Table 2), confirming the suitability of the MinP system for immobilizing recombinant proteins into PHA granules. Maximal release was observed for MinP-CueO at pH 9.0 (17 %) and for MinP-β-galactosidase at 37 °C (24 %) The latter was degraded after the treatment at 60 °C.

Additionally, the release of the fusion proteins was tested in the presence of different percentages of Triton X-100 (Fig. S3). A similar pattern than that observed for Bi1-G was obtained for the MinP-β-galactosidase, where 0.15 % (v/v) of detergent treatment yielded higher release of protein from the granules than the assay carried out at 1.5 % (v/v) of Triton X-100. However, in the case of MinP-CueO, both detergent percentages resulted in similar protein release. These results suggest that the release of MinP-fusions is not proportional to the detergent concentration and, together with those depicted in Fig. 5, indicate that the elution yields strongly

depend on the fused polypeptide and do not follow a simple trend with detergent concentration. This behaviour variety has also been found with the interaction of different BioF fusions with polyhydroxybutyrate granules (14) and suggests that detergent elution is a complex phenomenon involving both the affinity tag and the fused moiety that deserves a further molecular investigation.

To further validate the MinP tag system, the activity of each fusion enzyme was measured after treatment at different pHs (3.0, 5.0, 7.0 and 9.0) and temperatures (-20 °C, 4 °C, 37°C and 60 °C). As it can be observed in Fig. 8, immobilized MinP-β-galactosidase preserves the enzyme activity excepting at pH 3.0 (Fig. 8A) and 60 °C (Fig. 8B). Similar results were obtained with immobilized MinP-CueO (Fig. 8C-D), suggesting that either the proteins, the polymer support or both, are affected under these extreme conditions.

Finally, the functionalization ratio was calculated as explained above for both enzymes. The ratios of mg of protein per gram of PHA were of 16.8 ± 1.6 for MinP-β-galactosidase and 8.5 ± 0.4 for MinP-CueO. However, when calculated in molar terms, both proteins had similar functionalization ratios of 0.14 ± 0.03 μM per gram of PHA for MinP-β-galactosidase and 0.14 ± 0.06 μM per gram of PHA for MinP-CueO, consistent with the results for MinP-GFP (0.16 μM per gram of PHA).

DISCUSSION

This work addressed two main goals: to gain a better understanding on the binding capacity of BioF to the PHA granule and to use this knowledge to obtain improved versions of the tag that expands its biotechnological potential.

Many GAPs have been exploited as tags for the functionalization of PHA, especially PHA synthases and phasins. The mechanisms of the binding of these tags to the PHA material and the strength of the interaction are different, as well as the properties of each tag, making them suitable depending on the target application. Phasins constitute an attractive tool for tuning PHA materials due to their strong affinity to PHA. Despite that only a few studies have addressed the structural aspects of phasins, it is known that some common characteristics include the high proportion of disordered regions (28, 38), the presence of residues in α-helical conformation that increases in the presence of PHA (9, 28), and their tendency to form oligomers in solution (8, 28, 29, 39).

The PhaF phasin from *P. putida,* constitutes an attractive biotechnology tool, as its N-terminal domain (the BioF affinity tag) binds to PHA granules by non-specific hydrophobic interactions. In this work, various polypeptides based on BioF have been designed, differing in polarity, amphipaticity and length: Bi1, Bi2, Bi3 and Bi4 (Fig. 2). All of them, except Bi2, were able to bind *in vivo* to PHA granules, suggesting that substrate recognition does not reside in a specific region (Fig. 3). Bi2 was unable to bind to the granule, likely due to its short size preventing the establishment of sufficient hydrophobic interactions with the polymer. The binding of the BioF-based peptides to PHA granules was demonstrated to be independent of the presence of other GAPs such as phasins and depolymerase on the surface of the granule (Fig. 4). The presence

290 of PhaC1 and FadD could not be avoided due to their essential function for PHA accumulation,
291 but our results indicate that the presence of most of the GAPs is dispensable for BioF
292 segment binding.

293 The affinity of the truncated forms of the BioF tag to PHA was tested using various approaches.
294 The Bi3 displays a similar PHA localization pattern than BioF (Fig. 3B) although with a lower
295 binding strength (Fig. 5). On the other hand, and although localized predominantly on the PHA
296 granule surface by microscopy (Fig. 3A), the Bi4 segment did not show effective binding to
297 isolated PHA granules (Fig. 3B). Previous studies have demonstrated that the inclusion of a
298 functional leucine zipper motif is important for the oligomerization of PhaF (8, 28, 29).
299 However, as both Bi3 and Bi4 share the same leucine zipper region, these effects put into
300 question the crucial relevance of this motif for PHA affinity. Regarding the Bi1 fragment,
301 containing the BioF N-terminal region, it exhibited a PHA binding affinity similar to that of
302 whole BioF, whereas Bi3, containing the C-terminal region of BioF, displayed a reduced
303 binding strength, despite both peptides sharing a common region that corresponds to the Bi2
304 segment. This divergence could be attributed to the different hydrophobic and amphipathic
305 characteristics of both polypeptides (Fig. 1), rather than solely being a function of their
306 lengths. In fact, mean hydrophobicity seems to be a dominant factor for PHA binding more so
307 than amphipathicity, as the Bi1 fragment displays a clear higher value of $\langle H \rangle$ than Bi3, while it
308 presents only a moderate value for the hydrophobic moment $\langle \mu H \rangle$ (Fig. 2A). Moreover, Bi3 also
309 contains a region that is presumably natively unfolded in solution that may result in an increased
310 propensity for proteolytic attack (28). The two Bi3 bands observed in Fig. 3B may be due to this
311 feature.

312 The 48 amino acid segment Bi1 was chosen as an optimized tag for PHA functionalization and
313 was renamed MinP. Its binding capacity under different physicochemical conditions were
314 comparable or even stronger than full-length BioF (Fig. 3 - 5 and 6, 14, 29). The stability of
315 the binding between the tag and PHA is important to apply these devices across a variety
316 of physicochemical conditions, as many industrial processes take place at extreme temperatures
317 or pH (40, 41), conditions in which we demonstrate that MinP is retained at the surface of
318 the PHA granule (Fig. 5 and 6, table 2). The high stability of MinP on the surface of the PHA
319 granule constitutes a good choice for a strong immobilization of proteins and complements the
320 diversity of PHA affinity tags tailored to any need.

321 The amount of fusion protein attached to PHA granules was observed to be similar for BioF and
322 MinP, both in wild-type and Δ*pha+C1* strains (Table 1). Likewise, similar functionalization
323 in molar terms was obtained for MinP-CueO and MinP-β-galactosidase fusions. This suggests
324 that the PHA-binding capability of BioF mainly resides in its N-terminal moiety, and that the
325 presence of other GAPs on the surface of the granule does not impact in the functionalization
326 efficiency when the levels of the recombinant protein inside the cell are much higher than other
327 GAPs, as was previously observed (30).

328 Phasins have a positive effect on PHA production and PHA granule biogenesis (27, 31).
329 This has been proposed to be related with the interfacial role of phasins to segregate the
330 hydrophobic PHA granules away from hydrophilic cytoplasm, avoiding potential deleterious
331 effects of PHA production (42, 43). We observed the positive effects of the production
332 of phasin segments in Table 1, where presence of BioF increased the amount of PHA produced
333 in the Δ*pha+C1* strain, while MinP production did not. BioF tag presence likely favours

granule formation and thus improves the PHA production, whereas MinP appears to not have complete phasin activity. This could be due to the lack of the leucine zipper motif in MinP, which is important for oligomerization and to stablish the layer of GAPs that cover the PHA granule (29). Concerning the segregation of PHA granules, driven by the natural PhaF (27), it is affected in the absence of this protein, very likely influencing the PHA accumulation. This decrease in production could be solved by introducing the natural phasin PhaF if an industrial exploitation of the system that requires maximization of the PHA yield would be envisaged.

Finally, we propose a construction based on plasmid pSEVA238 to implement the production of fusion proteins at the C-terminal domain of MinP tag, and containing are movable linker as well as a MCS for cloning. The SEVA plasmids constitute a versatile platform for swapping modules as required (http://seva.cnb.csic.es/). The MinP module can be thus incorporated into the standardized synthetic biology library as a novel brick for polyester functionalization.

MATERIALS AND METHODS

Strains, media and growth conditions

The bacterial strains used in this study are listed in Table 3. *E. coli* and *P. putida* strains were grown routinely in Lysogeny Broth (LB) medium (44) at 37 °C and 30 °C, respectively, in a horizontal shaker at 200 rpm. Solid media were supplemented with 1.5 % (w/v) agar. Kanamycin antibiotic was added when needed at final concentration of 50 µg/mL.

For PHA production, the experiments were performed in 0.1 N M63 (13.6 g KH_2PO_4, 0.2 g $(NH_4)_2SO_4$, 0.5 mg $FeSO_4 \cdot 7\ H_2O$ to 1 L, adjusted to pH 7.0 with KOH) containing 15 mM sodium octanoate. This is a nitrogen limited medium for PHA production, where 0.1 N means a 10 % of the nitrogen source concentration of the standard M63 medium (2 g L^{-1}). A 20 mL overnight culture grown in LB at 30 ºC and 200 rpm was washed with 10 mL 145 mM NaCl, inoculated at OD_{600} 0.3 in 100 mL 0.1 N M63 medium and grown at 30 °C, as previously described (30). Minimal medium was supplemented with 1 mM $MgSO_4$ and a 0.1 mL of a solution of trace elements (for 1 L: 2.78 g $FeSO_4 \cdot 7H_2O$, 1.98 g $MnCl_2 \cdot 4H_2O$, 2.81 g $CoSO_4 \cdot 7H_2O$, 1.47 g $CaCl_2 \cdot 2H_2O$, 0.17 g $CuCl_2 \cdot 2H_2O$, 0.29 g $ZnSO_4 \cdot 7H_2O$ in 1 N HCl). When necessary, 3-methylbenzoate (3MB) was added in a final concentration of 1 mM for induction of pSEVA238 derivative plasmids (35).

365 ***DNA manipulation, plasmid and strain constructions***

366 DNA manipulations were performed as previously described (44) and the whole
367 oligonucleotides used are listed in Table 3.

368 For the construction of the strain carrying the PhaC1 polymerase, a modulable cluster
369 was *in silico* designed (Fig. 9). The synthesis was carried out by the GenBank® company.
370 The cluster allows the introduction of other modules through Gibson Assembly technique
371 (53) by using the overlap neutral regions *(*named as "*1, 2").* Besides, promoters and cargo
372 gene scan be easily exchanged using *Xba*I/*Xho*I/*BamH*I restriction sites. The cluster is
373 flanked by two *Not*I sites to be cloned into pTn7-M transposon for integration in *P.*
374 *putida* KT2440 *Δpha* genome. The *phaC1* gene was introduced under the control of a
375 constitutive synthetic promoter (P_{14a} promoter) (49), and the corresponding strain was
376 called *P. putida* KT2440 Δ*pha*+C1. The *M1-PhaC1-T0* module was synthetized
377 modifying the nucleotide sequence (Fig. S4) to avoid the restriction sites specified in Fig.
378 9 and introduced in the pTn7-Mplasmid for integration in *P. putida* KT2440 Δ*pha* genome
379 (Table 3).

380 For the construction of the pSMinPN plasmid, the sequence containing the *minP* gene
381 followed by a linker and flanked by *Xho*I restriction sites and a multiple cloning site (MCS)
382 was designed and synthetized. The construct was amplified using primers minPNt-F and
383 minPNt-R (Table 3) and cloned into pSEVA238 by using the *EcoR*I and *Hind*III restriction
384 enzymes. The gene coding for green fluoresce protein (GFP) was cloned into the pSMinPN
385 plasmid between the *Xho*I and *Hind*III sites to generate pSMinP-1 and transformed by
386 electroporation into *P. putida* KT2440 Δ*pha*+C1 (Table 3). For the construction of the
387 pSMinP-2 and pSMinP-3 plasmids, the genes coding for the β-galactosidase (*lacZ*) and

CueO (*cueO*) were amplified from pSEVA225 and pCueO respectively (Table 3), using the XhoI-LacZ-F and BamHI-LacZ-R oligonucleotides for *lacZ* and XhoI-CueO-F and HindIII-CueO-R for *cueO* (Table 3). Each one was cloned onto the 3' end of the MinP tag of pSMinPN plasmid between the *Xho*I /*BamH*I and *Xho*I / *Hind*III sites for *lac*Z and *cue*O respectively. Plasmids pSMinP-2 and pSMinP-3 were independently transferred by electroporation to *P. putida* KT2440 Δ*pha*+C1.

Protein structure prediction

All predicted α-helical sequences (18-aa windows) were analyzed for their hydrophobicity and amphipathicity with the *HeliQuest* utilities (http://heliquest.ipmc.cnrs.fr/) (34) using the Fauchere and Pliska scale (54) to calculate the mean hydrophobicity (⟨*H*⟩), while the mean hydrophobic moment (⟨μ*H*⟩) was calculated according to Eisenberg *et al*. (55). The hydrophobic moment is a measure of the amphipathicity of a helix where each amino acid is assigned a value (positive or negative) according to its hydrophobicity. Mean hydrophobicity is the sum of the hydrophobicity values divided by the number of residues (GenScript, s.f.).

BioF library construction

Based on structure prediction and hydropathic profile of BioF, several potential PHA affinity tags were constructed (Fig. 2). Different PCR products were obtained using the oligonucleotides Bio1-F and Bio1-R (Bi1)*;* Bio1-F and Bio4-R (BioF)*;* Bio2-F and Bio1-R (Bi2)*;* Bio3-F and Bio3-R (Bi4)*;* Bio2-F and Bio3-R (Bi3) with *P. putida* KT2440 genomic DNA as template (Table 3). The corresponding DNA fragments were cloned into pSP1plasmid (Table 3) using *Nde*I and *Hind*III restriction enzymes, giving the plasmids:

410 pSP1Bi1, pSP1Bi2, pSP1Bi3, pSP1Bi4 and pSP1BioF (Table 2). To allow the *in vivo*
411 localization of each BioF-derived polypeptide, the gene coding for the GFP was
412 amplified from pMAB20-GFP-LYTAG plasmid (31) by using the GFP-F and GFP-R
413 oligonucleotides (Table 3) and cloned onto the 3' end of the Bi-G segments between the
414 *Xho*I and *Hind*III restriction sites. The plasmids were finally transformed by
415 electroporation into *P. putida* KT2440. The most promising designs were also
416 introduced into *P. putida* KT2440 *Δpha*+C1.

417 ***Fluorescence microscopy***

418 Strains *P. putida* KT2440 and *P. putida* KT2440 *Δpha+C1* carrying the corresponding
419 plasmid: pSP1Bi1-G, pSP1Bi2-G, pSP1Bi3-G, pSP1Bi4-G or pSP1BioF-G (Table 3)
420 were grown in PHA producing media for 24 h at 30 ºC and 200 rpm. The induction
421 of the corresponding genes was carried out at OD_{600} 0.8 by the addition of 1 mM 3MB.
422 After 20 h of induction, the cells were directly observed through a Wide Field
423 Multidimensional Microscopy System Leica AF6000 LX, equipped with a CCD
424 Hamamatsu C9100-02 digital camera. Live cell imaging was performed using an 100x/AN
425 1.4 oil immersion, and GFP fluorescence was collected using a GFP-3035C-000 Semrock
426 filter, with excitation and emission ranges of 472/30 nm and 520/35 nm respectively, and
427 a 495 nm dichroic mirror.

428 ***PHA Granules isolation***

429 The PHA granules from *P. putida* KT2440 and *P. putida* KT2440 Δ*pha+C1* strains
430 carrying the corresponding plasmid: pSP1Bi1-G, pSP1Bi2-G, pSP1Bi3-G or pSP1BioF-
431 G were isolated following the protocol previously described (31). Briefly, bacterial cells

from a 14 mL of an OD_{600} 2-3 culture (except otherwise specified) were harvested by centrifugation at 12,000 x *g* for 20 min, suspended in 7 mL of 15 mM Tris HCl pH 8.0, and disrupted twice by French Press (1,000 psi). The resulting suspension was centrifuged 30 min at 12,000 x *g*, and the pellet fraction was resuspended in 5 mL of 15 mM Tris HCl pH 8.0 and layered over 5 mL of 55 % glycerol. The solution was centrifuged at 17,000 x *g* for 30 min, and the isolated granules were washed twice with 15 mM Tris HCl pH 8.0 to remove the residual glycerol, and suspended into 0.5-1.5 mL of 15 mM Tris HCl pH 8.0.

Stability of MinP-proteins attached to the PHA granule

An aliquot of 100 µL of the isolated granules from KT2440 Δ*pha+C1* (see *PHA granules isolation*) containing the plasmid coding for the corresponding BioF-derived polypeptide were collected by centrifugation, suspended in Triton X-100 at different concentrations (0.015 %, 0.15 %, 1.5 % in 15 mM Tris HCl pH 8.0, v/v) and incubated for 2 h at room temperature. The assay was later repeated with the final fusion proteins MinP-CueO and MinP-β-galactosidase.

The binding stability of Bi1-G protein, MinP-CueO and MinP-β-galactosidase to the PHA granules was also tested under different temperature, pH and ionic strength conditions as previously described (29). Briefly, an aliquot of 100 µL of purified granules from *P. putida* KT2440 Δ*pha+C1* (pSP1Bi1-G, pSPMinP-2 and pSPMinP-3) (see *PHA granules isolation*) was incubated for 2 h (i) in 100 µL of 15 mM Tris HCl pH 8.0 at different temperatures: -20, 4, 37 or 60 °C; (ii) in 100 µL of 0, 10, 100, 1000 mM NaCl, at 4 °C; (iii) in 100 µL of 15 mM sodium citrate pH 3.0 or 5.0, in 100 µL of 15 mM Tris-HCl pH 7.0 or 9.0, at 4 °C. In all cases after the 2 h of incubation time, the granules were

455 centrifuged at 12,000 × *g* for 15 min at 4 °C and the retained and soluble protein fractions
456 were analyzed and estimated by SDS-PAGE as specified bellow. The percentage of
457 discharged protein was obtained by subtracting the amount of protein liberated from the
458 granules from the total amount of protein (sum of the soluble and insoluble fractions).
459 Every assay was performed in duplicate.

460 ***Protein Quantification***

461 The content of the different BioF and MinP-based-tag proteins on the granule surface was
462 determined by imaging the bands separated on 12.5 % SDS-PAGE and estimating the
463 amount of protein present using the software package *ImageJ*. Pellet and granule protein
464 fractions of the crude extract and the granule fraction isolated from each culture were
465 separated by SDS-PAGE and stained with Coomassie brilliant blue G-250 following the
466 described protocol (44). The amount of protein anchored to the surface of the granules
467 was estimated by imaging the Coomassie stained gels and taking into account the amount
468 of isolated granules loaded in each well and calibrating against Precision Plus Protein
469 Standards from BioRad®.

470 ***PHA quantification***

471 Monomer composition and cellular content of PHA were determined by gas
472 chromatography-mass spectrometry (GC-MS) following the previously described protocol
473 (56). Briefly, PHA monomers were obtained by acid methanolysis with 2 mL of methanol
474 acidified with 15 % H_2SO_4 (v/v) and 2 mL of 0.5 mg/mL of 3-methyl benzoate in
475 chloroform as an internal standard. This mixture was incubated for 5 h in an oil bath at
476 100 °C. After cooling, 1 mL of distilled water was added to the mixture and centrifuged

for 10 min at 3,000 x *g* to separate the phases. A second step of extraction was performed to remove the residual H_2SO_4. Finally, a small amount of Na_2SO_4 powder was added toremove residual water. The organic layer was analyzed using an Agilent 7890A GC equipped with a DB-5HT capillary column (30 m length, 0.25 mm internal diameter, 0. 1µm film thickness), and mass data were acquired and processed with an Agilent 5975C mass spectrometer. The oven temperature program was set at an initial temperature of 80 °C for 2 min, then from 80 °C up to 115 °C at a rate of 5 °C/min for efficient separation of peaks. Spectra were obtained as electron impacts with an ionizing energy for MS operation of 70 eV.

Biomass calculation was carried out as previously described (56). Fifty millilitres of culture medium was centrifuged for 30 min at 3,000 x *g* at 4 °C and pellets were lyophilized for 24 h and weighed.

Enzymatic activity assays

Enzymatic activity was tested for the granule-immobilized fusion proteins after treatment at different pHs and temperature, and its relative activity was calculated regarding untreated granule-immobilized enzymes as follows:

β-galactosidase assay.

Firstly, in order to determine specific activity (SA) of the immobilized enzyme, an aliquot of 12.5 µL of granules with a defined protein concentration (see *PHA granules isolation and Protein quantification sections*), was centrifuged (15 min, 16,060 x *g*, RT) and resuspended in 500 µL of 100 mM sodium phosphate pH 7.0 in 2 mL tubes, to which 500 µL of Buffer Z (Na_2HPO_4 60 mM, NaH_2PO_4 40 mM, KCl 10 mM, $MgSO_4$ 1 mM, β-

499 mercaptoethanol 50 mM, pH 7.0) were added. The tubes were pre-warmed at 28 ºC for 3
500 min in a thermoblock (Fisher Scientific, USA) and subsequently, 200 µL of *O*-nitrophenyl-
501 β-galactopyranoside (ONPG) (Sigma-Aldrich, USA) (4 $mg \cdot mL^{-1}$) were added and
502 incubated for 3 min more, after which the reaction was stopped by the addition of 500 µL
503 1 M Na_2CO_3, pH 11.0. Previously, we had determined both the protein concentration and
504 the reaction time needed to measure the activity in the linear part of the activity curve. The
505 ONP generated in the stopped reaction was measured at 420 nm in a spectrophotometer
506 (DU®520, Beckman) and used for the SA calculation (units per mg of protein), by using
507 an extinction coefficient of 4800 M^{-1} cm^{-1} for ONP. The SA of the immobilized MinP-β-
508 galactosidase resulted to be 6,8 x 10^4 UA mg^{-1}, in agreement with the SA reported for BioF-β-
509 galactosidase (2,8 x 10^5 UA mg^{-1}) (30). One unit of activity, UA, is defined as the amount
510 of protein needed to hydrolyze 1 nmol of ONPG per min at 28 ºC.

511 For the functional stability test, the granules containing the immobilized protein were
512 previously treated as described in *stability of MinP-proteins attached to PHA granules*
513 section (2 h at pH 3.0, 5.0, 7.0 or 9.0 and temperatures -20 °C, 4 °C, 37°C or 60 °C).
514 Positive control was prepared with granules at pH 7.0 and at 4 ºC for pH and temperature
515 treatment respectively. As negative control, granules extracted from the parental strain *P.*
516 *putida* KT2440 Δ*pha* + C1 incubated at 4 ºC for 2 h were taken. The enzyme activity assay
517 was undertaken as explained in the above paragraph except that, after stopping the reaction,
518 and for the ONP quantification, an aliquot of 200 µL of each suspension was transferred
519 to a multiwell plate (Falcon, USA) and the absorbance at 420 nm was measured in a
520 VersaMax microplate reader (Molecular Devices). Enzyme activity was calculated as
521 Miller Units by using the following formula: 1000 x (OD_{420}) / (T x P) where T is the

522 reaction time in min; and P is the total amount of protein quantified by gel densitometry
523 after the treatment (see *Protein quantification section*). The enzyme activity in each case
524 was shown as percentage with regard to a control at pH 7.0 for the pH treatments, and at 4
525 ºC for the temperature treatments.

526 *CueO assay*

527 In order to determine SA of the immobilized enzyme, an aliquot of 50 µL of granules (see
528 *PHA granules isolation*) with a defined protein concentration as determined by gel
529 densitometry, was centrifuged (15 min, 16,060 x *g* at room temperature) and resuspended
530 in in the same volume of 100 mM sodium phosphate pH 6.5. The granules suspension was
531 transferred to a spectrophotometer cuvette and the reaction was triggered by the addition
532 of $CuCl_2$ (Fluka, Switzerland) and the CueO substrate 2,6 dimethoxyphenol (DMP)
533 (Sigma-Aldrich, USA) at a final concentration of 10 µM and 2 mM respectively in 100
534 mM sodium phosphate pH 6.5 and in a final volume of 1 ml. The reaction product,
535 3,3′,5,5′-tetramethoxydiphenoquinone, was followed at 30 ºC by measuring the
536 absorbance at 468 nm (ε_{468nm} = 14 800 M^{-1} cm^{-1}) (48) each 5 min in order to be sure to
537 determine the activity in the linear part of the oxidation curve. The specific activity of the
538 immobilized MinP-CueO resulted to be 2 300 UA mg^{-1}, comparable with that of soluble
539 CueO (6 000 UA mg^{-1}), although slightly reduced probably due to the presence of the MinP
540 fused moiety. One UA is defined as the amount of enzyme needed to oxidize 1 nmol of
541 DMP per min and at 30 ºC.

542 For the functional stability test, the granules containing the immobilized protein were
543 previously treated as described in *stability of MinP-proteins attached to PHA granules*
544 section (2 h at pH 3.0, 5.0, 7.0 or 9.0 and temperatures -20 °C, 4 °C, 37°C or 60 °C).

Positive control was prepared with granules at pH 7.0 and at 4 ºC for pH and temperature treatment respectively. As negative control, granules with heat-inactivated MinP-CueO (2 min, 98 ºC) were used. For relative quantification, the assays were carried out in a multiwell plate (Falcon, USA) in a final volume of 200 µL and the activity monitored in a multiwell reader at OD_{468} (VersaMax, Molecular devices).

ACKNOWLEDGEMENTS

This work was supported by the European Union's Horizon 2020 Research and Innovation Programme, grant agreement no. 633962 (P4SB), the Spanish Ministry of Science, Innovation and Universities (BIO2017-83448-R, BIO2016-79323-R, RTI2018-094564-B-I00) and the Community of Madrid (P2013/MIT2807, P2018/NMT4389). Francisco Blanco is a recipient of a predoctoral grant from the State Program for the Promotion of Talent and its Employability in R&D&I (PRE-2018-083859) from the Spanish Ministry of Science and Innovation.

REFERENCES

1. Hay ID, Du J, Burr N, Rehm BHA. 2015. Bioengineering of bacteria to assemble custom-made polyester affinity resins. Appl Environ Microbiol 81:282-91.
2. Li Z, Loh XJ. 2017. Recent advances of using polyhydroxyalkanoate-based nanovehicles as therapeutic delivery carriers. WIREs Nanomed Nanobiotechnol 9.
3. Barbosa O, Ortiz C, Berenguer-Murcia A, Torres R, Rodrigues RC, Fernandez-Lafuente R. 2015. Strategies for the one-step immobilization-purification of enzymes as industrial biocatalysts. Biotechnol Adv 33:435-56.
4. Tortajada M, da Silva LF, Prieto MA. 2013. Second-generation functionalized medium-chain-length polyhydroxyalkanoates: the gateway to high-value bioplastic applications. Int Microbiol 16:1-15.
5. Jendrossek D, Pfeiffer D. 2014. New insights in the formation of polyhydroxyalkanoate granules (carbonosomes) and novel functions of poly(3-hydroxybutyrate). Environ Microbiol 16:2357-73.
6. Parlane NA, Gupta SK, Rubio-Reyes P, Chen S, Gonzalez-Miro M, Wedlock DN, Rehm BHA. 2017. Self-Assembled Protein-Coated Polyhydroxyalkanoate Beads: Properties and Biomedical Applications. ACS Biomater Sci Eng 3:3043-57.
7. Dinjaski N, Prieto MA. 2015. Smart polyhydroxyalkanoate nanobeads by protein based functionalization. Nanomedicine 11:885-99.
8. Maestro B, Sanz JM. 2017. Polyhydroxyalkanoate-associated phasins as phylogenetically heterogeneous, multipurpose proteins. Microb Biotechnol 10:1323-37.
9. Mezzina MP, Pettinari MJ. 2016. Phasins, Multifaceted Polyhydroxyalkanoate Granule-

Associated Proteins. Appl Environ Microbiol 82:5060-7.

10. Li J, Shang G, You M, Peng S, Wang Z, Wu H, Chen GQ. 2011. Endotoxin removing method based on lipopolysaccharide binding protein and polyhydroxyalkanoate binding protein PhaP. Biomacromolecules 12:602-8.

11. Banki MR, Gerngross TU, Wood DW. 2005. Novel and economical purification of recombinant proteins: intein-mediated protein purification using *in vivo* polyhydroxybutyrate (PHB) matrix association. Protein Sci 14:1387-95.

12. Wang Z, Wu H, Chen J, Zhang J, Yao Y, Chen GQ. 2008. A novel self-cleaving phasin tag for purification of recombinant proteins based on hydrophobic polyhydroxyalkanoate nanoparticles. Lab Chip 8:1957-62.

13. Geng Y, Wang S, Qi Q. 2010. Expression of active recombinant human tissue-type plasminogen activator by using *in vivo* polyhydroxybutyrate granule display. Appl Environ Microbiol 76:7226-30.

14. Bello-Gil D, Maestro B, Fonseca J, Dinjaski N, Prieto MA, Sanz JM. 2018. Poly-3-Hydroxybutyrate Functionalization with BioF-Tagged Recombinant Proteins. Appl Environ Microbiol 84.

15. Bello-Gil D, Roig-Molina E, Fonseca J, Sarmiento-Ferrandez MD, Ferrandiz M, Franco E, Mira E, Maestro B, Sanz JM. 2018. An enzymatic system for decolorization of wastewater dyes using immobilized CueO laccase-like multicopper oxidase on poly-3-hydroxybutyrate. Microb Biotechnol 11:881-92.

16. Wong JX, Ogura K, Chen S, Rehm BHA. 2020. Bioengineered Polyhydroxyalkanoates as Immobilized Enzyme Scaffolds for Industrial Applications. Front Bioeng Biotechnol 8:156.

17. Moldes C, Farinos GP, de Eugenio LI, Garcia P, Garcia JL, Ortego F, Hernandez-Crespo

603 P, Castanera P, Prieto MA. 2006. New tool for spreading proteins to the environment:
604 Cry1Ab toxin immobilized to bioplastics. Appl Microbiol Biotechnol 72:88-93.
605 18. Backstrom BT, Brockelbank JA, Rehm BH. 2007. Recombinant *Escherichia coli* produces
606 tailor-made biopolyester granules for applications in fluorescence activated cell sorting:
607 functional display of the mouse interleukin-2 and myelin oligodendrocyte glycoprotein.
608 BMC Biotechnol 7:3.
609 19. Atwood JA, Rehm BH. 2009. Protein engineering towards biotechnological production of
610 bifunctional polyester beads. Biotechnol Lett 31:131-7.
611 20. Yao YC, Zhan XY, Zhang J, Zou XH, Wang ZH, Xiong YC, Chen J, Chen GQ. 2008. A
612 specific drug targeting system based on polyhydroxyalkanoate granule binding protein
613 PhaP fused with targeted cell ligands. Biomaterials 29:4823-30.
614 21. Dong Y, Li P, Chen CB, Wang ZH, Ma P, Chen GQ. 2010. The improvement of fibroblast
615 growth on hydrophobic biopolyesters by coating with polyhydroxyalkanoate granule
616 binding protein PhaP fused with cell adhesion motif RGD. Biomaterials 31:8921-30.
617 22. You M, Peng G, Li J, Ma P, Wang Z, Shu W, Peng S, Chen GQ. 2011. Chondrogenic
618 differentiation of human bone marrow mesenchymal stem cells on polyhydroxyalkanoate
619 (PHA) scaffolds coated with PHA granule binding protein PhaP fused with RGD peptide.
620 Biomaterials 32:2305-13.
621 23. Xie H, Li J, Li L, Dong Y, Chen GQ, Chen KC. 2013. Enhanced proliferation and
622 differentiation of neural stem cells grown on PHA films coated with recombinant fusion
623 proteins. Acta Biomater 9:7845-54.
624 24. Fan F, Wang L, Ouyang Z, Wen Y, Lu X. 2018. Development and optimization of a tumor
625 targeting system based on microbial synthesized PHA biopolymers and PhaP mediated

functional modification. Appl Microbiol Biotechnol 102:3229-41.

25. Xue Q, Liu XB, Lao YH, Wu LP, Wang D, Zuo ZQ, Chen JY, Hou J, Bei YY, Wu XF, Leong KW, Xiang H, Han J. 2018. Anti-infective biomaterials with surface-decorated tachyplesin I. Biomaterials 178:351-362.

26. Prieto MA, Buhler B, Jung K, Witholt B, Kessler B. 1999. PhaF, a polyhydroxyalkanoate-granule-associated protein of *Pseudomonas oleovorans* GPo1 involved in the regulatory expression system for pha genes. J Bacteriol 181:858-68.

27. Galan B, Dinjaski N, Maestro B, de Eugenio LI, Escapa IF, Sanz JM, Garcia JL, Prieto MA. 2011. Nucleoid-associated PhaF phasin drives intracellular location and segregation of polyhydroxyalkanoate granules in *Pseudomonas putida* KT2442. Mol Microbiol 79:402-18.

28. Maestro B, Galan B, Alfonso C, Rivas G, Prieto MA, Sanz JM. 2013. A new family of intrinsically disordered proteins: structural characterization of the major phasin PhaF from *Pseudomonas putida* KT2440. PLoS One 8:e56904.

29. Tarazona NA, Maestro B, Revelles O, Sanz JM, Prieto MA. 2019. Role of leucine zipper-like motifs in the oligomerization of *Pseudomonas putida* phasins. Biochim Biophys Acta Gen Subj 1863:362-70.

30. Moldes C, Garcia P, Garcia JL, Prieto MA. 2004. *In vivo* immobilization of fusion proteins on bioplastics by the novel tag BioF. Appl Environ Microbiol 70:3205-12.

31. Dinjaski N, Prieto MA. 2013. Swapping of phasin modules to optimize the *in vivo* immobilization of proteins to medium-chain-length polyhydroxyalkanoate granules in *Pseudomonas putida*. Biomacromolecules 14:3285-93.

32. Mato A, Tarazona NA, Hidalgo A, Cruz A, Jimenez M, Perez-Gil J, Prieto MA. 2019.

649 Interfacial Activity of Phasin PhaF from *Pseudomonas putida* KT2440 at Hydrophobic-
650 Hydrophilic Biointerfaces. Langmuir 35:678-686.
651 33. Terpe K. 2003. Overview of tag protein fusions: from molecular and biochemical
652 fundamentals to commercial systems. Appl Microbiol Biotechnol 60:523-33.
653 34. Gautier R, Douguet D, Antonny B, Drin G. 2008. HELIQUEST: a web server to screen
654 sequences with specific alpha-helical properties. Bioinformatics 24:2101-2.
655 35. Silva-Rocha R, Martinez-Garcia E, Calles B, Chavarria M, Arce-Rodriguez A, de Las Heras
656 A, Paez-Espino AD, Durante-Rodriguez G, Kim J, Nikel PI, Platero R, de Lorenzo V. 2013.
657 The Standard European Vector Architecture (SEVA): a coherent platform for the analysis
658 and deployment of complex prokaryotic phenotypes. Nucleic Acids Res 41:D666-75.
659 36. Husain Q. 2010. β Galactosidases and their potential applications: a review. Crit Rev
660 Biotechnol 30:41-62.
661 37. Patel N, Shahane S, Shivam, Majumdar R, Mishra U. 2019. Mode of Action, Properties,
662 Production, and Application of Laccase: A Review. Recent Pat Biotechnol 13:19-32.
663 38. Mezzina MP, Wetzler DE, Catone MV, Bucci H, Di Paola M, Pettinari MJ. 2014. A phasin
664 with many faces: structural insights on PhaP from Azotobacter sp. FA8. PLoS One
665 9:e103012.
666 39. Zhao H, Wei H, Liu X, Yao Z, Xu M, Wei D, Wang J, Wang X, Chen GQ. 2016. Structural
667 Insights on PHA Binding Protein PhaP from *Aeromonas hydrophila*. Sci Rep 6:39424.
668 40. Littlechild JA. 2015. Enzymes from Extreme Environments and Their Industrial
669 Applications. Front Bioeng Biotechnol 3:161.
670 41. Sarmiento F, Peralta R, Blamey JM. 2015. Cold and Hot Extremozymes: Industrial
671 Relevance and Current Trends. Front Bioeng Biotechnol 3:148.

672 42. Wieczorek R, Pries A, Steinbuchel A, Mayer F. 1995. Analysis of a 24-kilodalton protein
673 associated with the polyhydroxyalkanoic acid granules in *Alcaligenes eutrophus*. J
674 Bacteriol 177:2425-35.
675 43. Mezzina MP, Wetzler DE, de Almeida A, Dinjaski N, Prieto MA, Pettinari MJ. 2015. A
676 phasin with extra talents: a polyhydroxyalkanoate granule-associated protein has chaperone
677 activity. Environ Microbiol 17:1765-76.
678 44. Sambrook J. 2001. Molecular cloning : a laboratory manual / Joseph Sambrook, David W.
679 Russell. Cold Spring Harbor Laboratory, Cold Spring Harbor, N.Y.
680 45. Bagdasarian M, Lurz R, Ruckert B, Franklin FC, Bagdasarian MM, Frey J, Timmis KN.
681 1981. Specific-purpose plasmid cloning vectors. II. Broad host range, high copy number,
682 RSF1010-derived vectors, and a host-vector system for gene cloning in Pseudomonas. Gene
683 16:237-47.
684 46. Boyer HW, Roulland-Dussoix D. 1969. A complementation analysis of the restriction and
685 modification of DNA in *Escherichia coli*. J Mol Biol 41:459-72.
686 47. Herrero M, de Lorenzo V, Timmis KN. 1990. Transposon vectors containing non-antibiotic
687 resistance selection markers for cloning and stable chromosomal insertion of foreign genes
688 in gram-negative bacteria. J Bacteriol 172:6557-67.
689 48. Grass G, Rensing C. 2001. CueO is a multi-copper oxidase that confers copper tolerance in
690 *Escherichia coli*. Biochem Biophys Res Commun 286:902-8.
691 49. Zobel S, Benedetti I, Eisenbach L, de Lorenzo V, Wierckx N, Blank LM. 2015. Tn7-Based
692 Device for Calibrated Heterologous Gene Expression in *Pseudomonas putida*. ACS Synth
693 Biol 4:1341-51.
694 50. Pais J, Farinha I, Freitas F, Serafim LS, Martinez V, Martinez JC, Arevalo-Rodriguez M,

695 Auxiliadora Prieto M, Reis MA. 2014. Improvement on the yield of polyhydroxyalkanotes
696 production from cheese whey by a recombinant *Escherichia coli* strain using the proton
697 suicide methodology. Enzyme Microb Technol 55:151-8.
698 51. Kessler B, de Lorenzo V, Timmis KN. 1992. A general system to integrate lacZ fusions
699 into the chromosomes of gram-negative eubacteria: regulation of the Pm promoter of the
700 TOL plasmid studied with all controlling elements in monocopy. Mol Gen Genet 233:293-
701 301.
702 52. Choi KH, Gaynor JB, White KG, Lopez C, Bosio CM, Karkhoff-Schweizer RR, Schweizer
703 HP. 2005. A Tn7-based broad-range bacterial cloning and expression system. Nat Methods
704 2:443-8.
705 53. Iverson SV, Haddock TL, Beal J, Densmore DM. 2016. CIDAR MoClo: Improved MoClo
706 Assembly Standard and New *E. coli* Part Library Enable Rapid Combinatorial Design for
707 Synthetic and Traditional Biology. ACS Synth Biol 5:99-103.
708 54. Fauchère JL, Pliska V. 1986. Reply from Fauchère and Pliska. Trends in Biochemical
709 Sciences 11:70.
710 55. Eisenberg D, Weiss RM, Terwilliger TC. 1982. The helical hydrophobic moment: a
711 measure of the amphiphilicity of a helix. Nature 299:371-4.
712 56. de Eugenio LI, Escapa IF, Morales V, Dinjaski N, Galan B, Garcia JL, Prieto MA. 2010.
713 The turnover of medium-chain-length polyhydroxyalkanoates in *Pseudomonas putida*
714 KT2442 and the fundamental role of PhaZ depolymerase for the metabolic balance. Environ
715 Microbiol 12:207-21.

716

Figures leyend

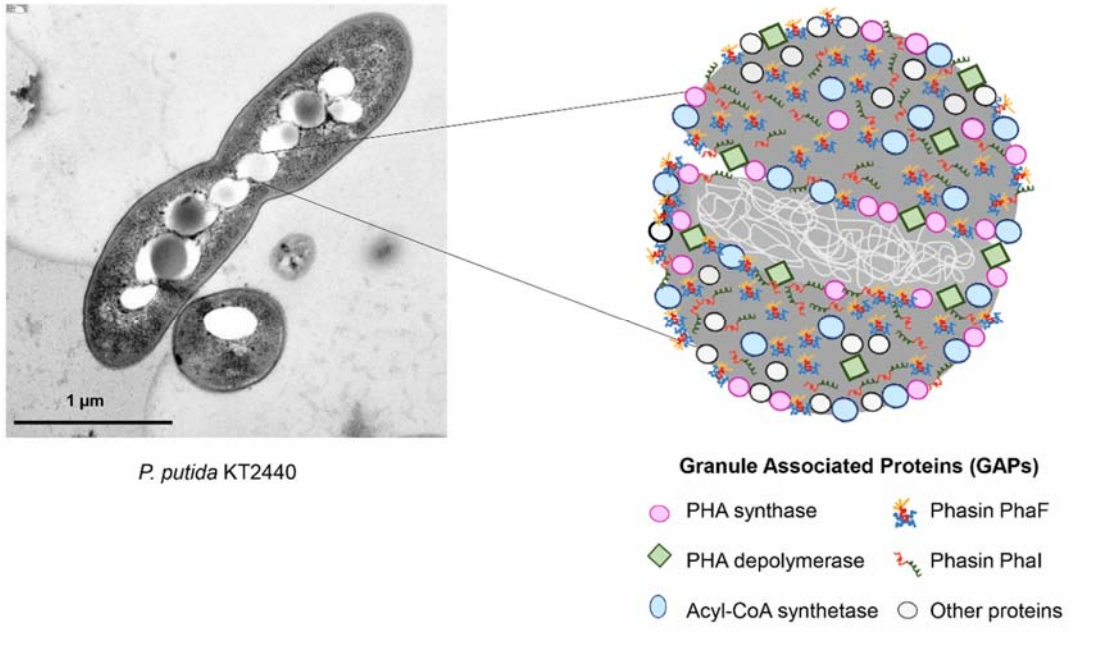

Fig 1. PHA production and granule structure. A) TEM image of *P. putida* KT2440 growing under PHA producing conditions. Granules are accumulated as hydrophobic inclusions inside the cell. B) Schematic representation of the PHA granule from *P. putida* KT2440. The PHA is surrounded by a layer of proteins called granule associated proteins (GAPs) such as PHA polymerase, depolymerase and phasins.

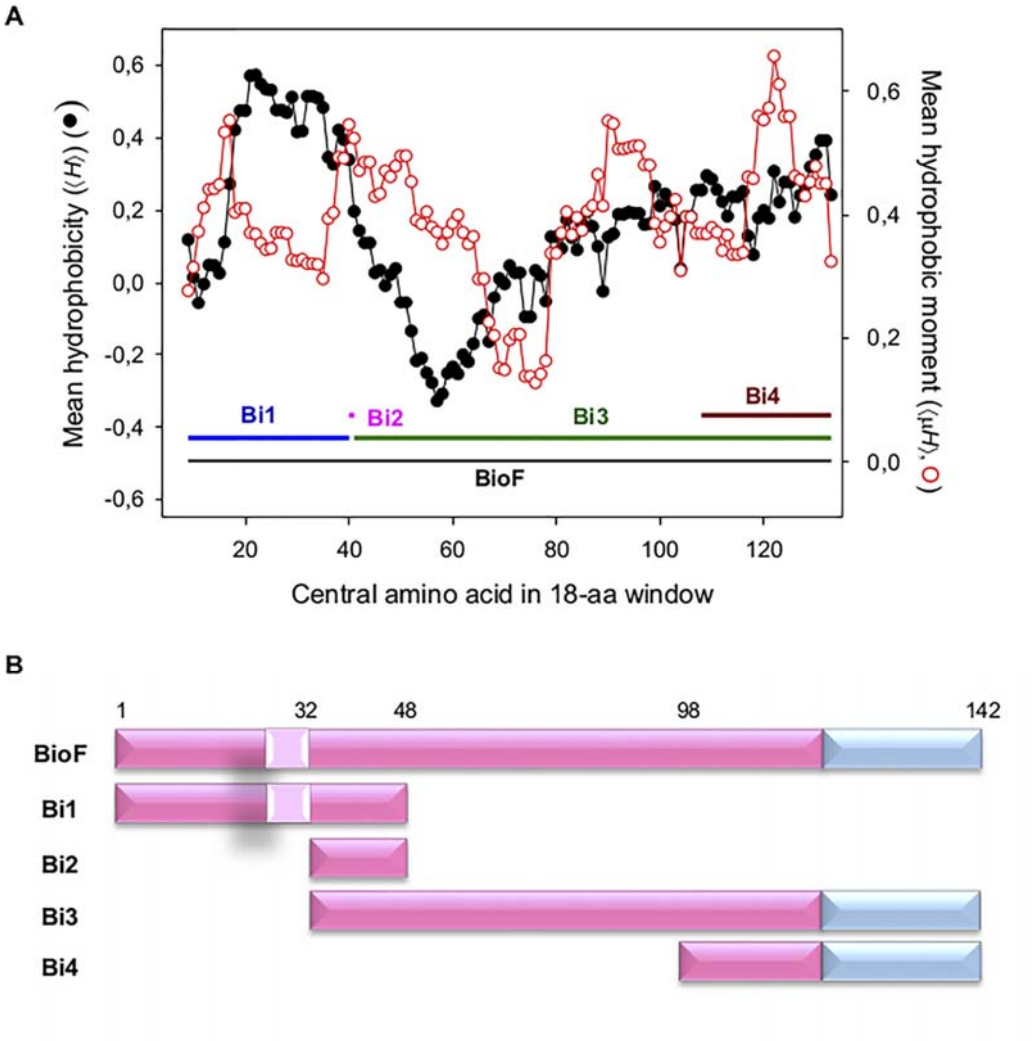

727

728 **Fig 2. Evaluation of the structural aspects of the N-terminal domain of phasin PhaF(BioF)**
729 **and design of a set of BioF-based fragments.** A) Analysis of mean hydrophobicity(⟨*H*⟩) and
730 mean hydrophobic moment (⟨μ*H*⟩) of predicted α-helical stretches within the PHA binding
731 and leucine zipper motifs of PhaF. Calculations were performed with the *HeliQues*t utilities
732 using a sequence window size of 18 aa (34). B) Schematic representation of the battery of BioF-
733 based peptides designed. BioF amino acid residue positions are indicated above, pink
734 corresponds to the N-terminal domain of PhaF, light pink corresponds to the conserved highly
735 hydrophobic motif (WLAGLGI), blue corresponds to the central leucine zipper motif.

736

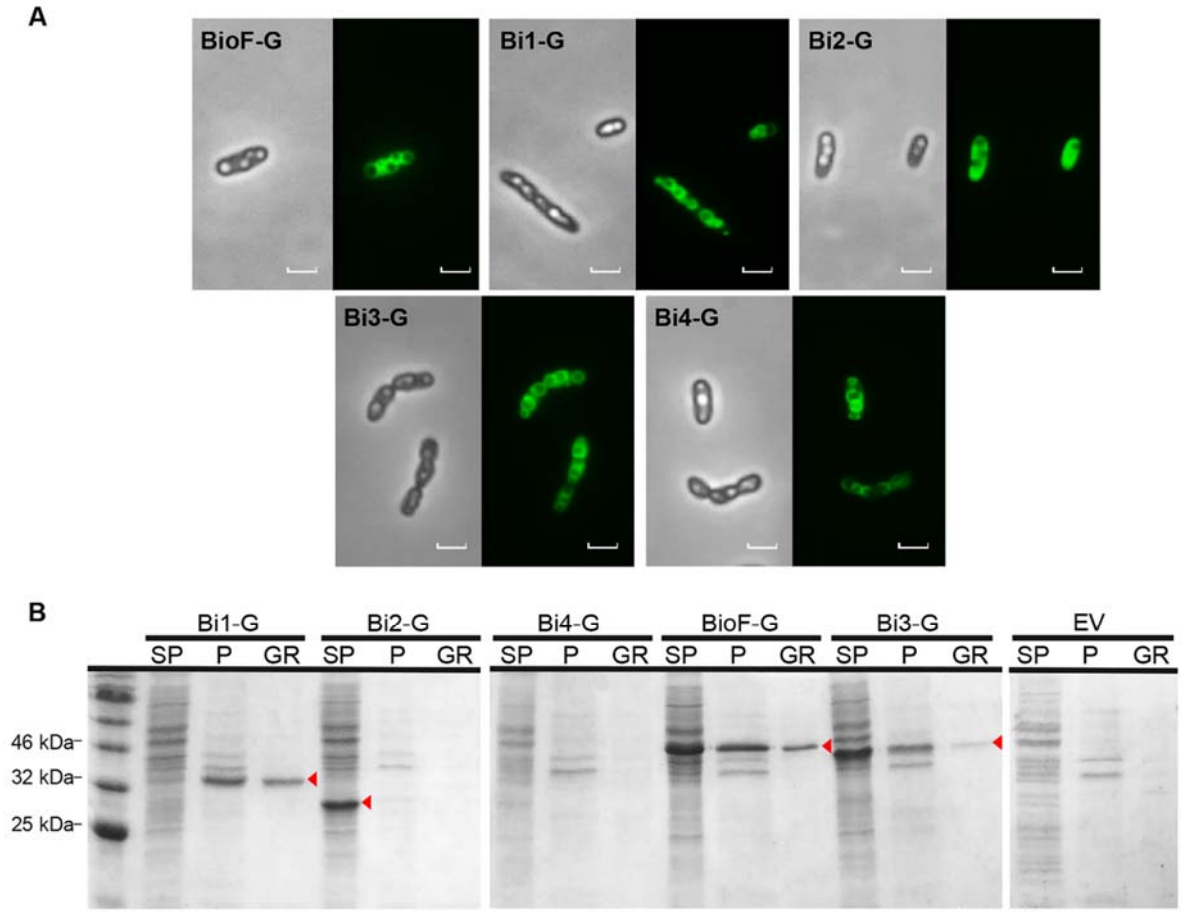

737

738 **Fig 3.** Localization of the different Bi segment-GFP fusion proteins in *P. putida* KT2440 after
739 24 h of growth in 0.1 N M63 plus 15 mM of octanoate, induced at $O.D._{600}$ 0.8 with 1 mM of
740 3-MB. BioF-G: *P. putida* KT2440 (pSP1BioF-G); Bi1-G: *P. putida* KT2440 (pSP1Bi1-G); Bi2-
741 G: *P. putida* KT2440 (pSP1Bi2-G); Bi3-G: *P. putida* KT2440 (pSP1Bi3-G); Bi4: *P. putida*
742 KT2440 (pSP1Bi4-G). A) *In vivo* localization of BioF-based tag segments fused to GFP by
743 epifluorescence and phase contrast microscopy. Scale bars mean 2 µm. B) SDS-PAGE stained
744 with Coomassie brilliant blue. The lanes contain the fractions isolated (SP: crude extract

supernatant, P: crude extract pellet, GR: isolated PHA granules). EV: *P. putida* KT2440 (pSP1) empty vector. The volume loaded in each well was 15 µL. Red arrows indicate the predicted molecular weights of the recombinant proteins.

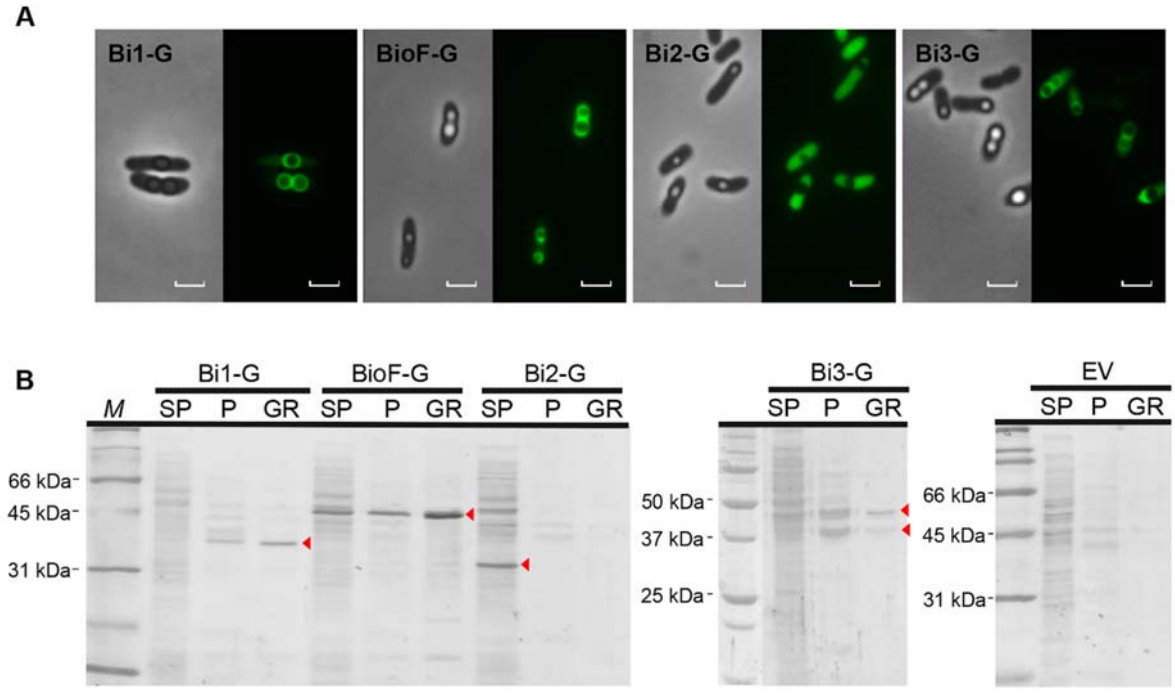

Fig 4. Localization of the different Bi segment-GFP fusion proteins in *P. putida* KT2440 *Δpha+C1* after 24 h of growth in 0.1 N M63 plus 15 mM of octanoate, induced at $O.D._{600}$ 0.8 with 1 mM of 3-MB. Bi1-G: *P. putida* KT2440 *Δpha+C1* (pSP1Bi1-G); Bi2-G: *P. putida* KT2440 *Δpha+C1* (pSP1Bi2-G); BioF-G: *P. putida* KT2440 *Δpha+C1* (pSP1BioF-G); Bi3-G: *P. putida* KT2440 *Δpha+C1* (pSP1Bi3-G). A) *In vivo* localization of BioF-based tag segments fused to GFP by epifluorescence and phase contrast microscopy. Scale bars mean 2 µm. B) SDS-PAGE stained with Coomassie brilliant blue. The lanes contain the fractions isolated (SP:

crude extract supernatant, P: crude extract pellet, GR: isolated PHA granules). EV: *P. putida* KT2440 *Δpha+C1* (pSP1) empty vector. The volume loaded in each well was 15 µL. Red arrows indicate the predicted molecular weights of the recombinant proteins.

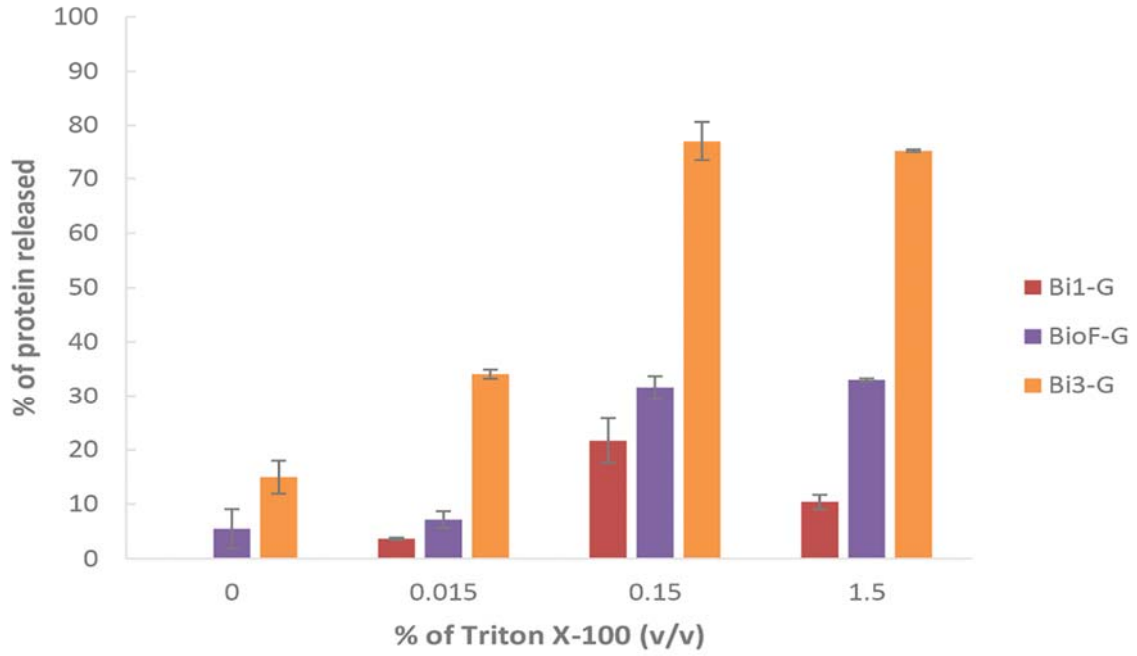

Fig 5. Percentage of protein released from isolated PHA granules of *P. putida* KT2440 Δ*pha+C1* (pSP1Bi1-G), *P. putida* KT2440 Δ*pha+C1* (pSP1BioF-G) and *P. putida* KT2440 Δ*pha+C1* (pSP1Bi3-G) after treatment for 2 h with various concentrations of Triton X-100 at room temperature and separating released (supernatant) and PHA-bound protein (pellet). Percentages refer to the ratio between soluble fraction to the total amount of protein (sum of soluble and insoluble fractions) using *ImageJ* to quantitate band intensities on Coomassie-

stained SDS-PAGE. Error bars represent the SD from three biological replicates and two technical each.

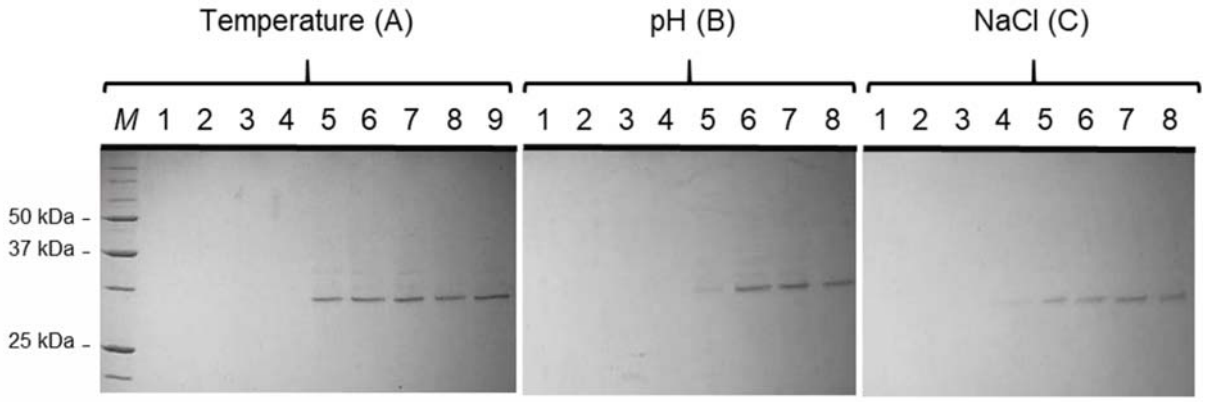

Fig 6. Coomassie stained SDS-PAGE of PHA granules extracted from *P. putida* KT2440 Δ*pha*+C1 producing Bi1-G. The stability of Bi1-G interacting with PHA granules was assessed by exposure a range of temperatures (A), pH (B) and ionic strength (C) for 2 h. A) Lanes 1-4, released soluble fraction after at -20 °C, 4 °C, 37 °C and 60 °C, respectively. Lanes 5-8, PHA granule retained protein fraction after treatment at -20 °C, 4 °C, 37 °C and 60 °C, respectively; Lane 9, untreated isolated granules. B) Lanes 1-4, released soluble fraction after treatment with pH 3.0, 5.0, 7.0 and 9.0, respectively. Lanes 5-8, PHA granule retained protein fraction after treatment at pH 3.0, 5.0, 7.0 and 9.0, respectively. C) Lanes 1-4, released soluble fraction after treatment with 0,10, 100 and 1000 mM NaCl, respectively. Lanes 5-8, PHA granule retained protein fraction after treatment with 0, 10, 100 and 1000 mM NaCl, respectively. Volumes loaded correspond to 15 µL of the soluble and insoluble fractions obtained after the treatment of the granules.

784

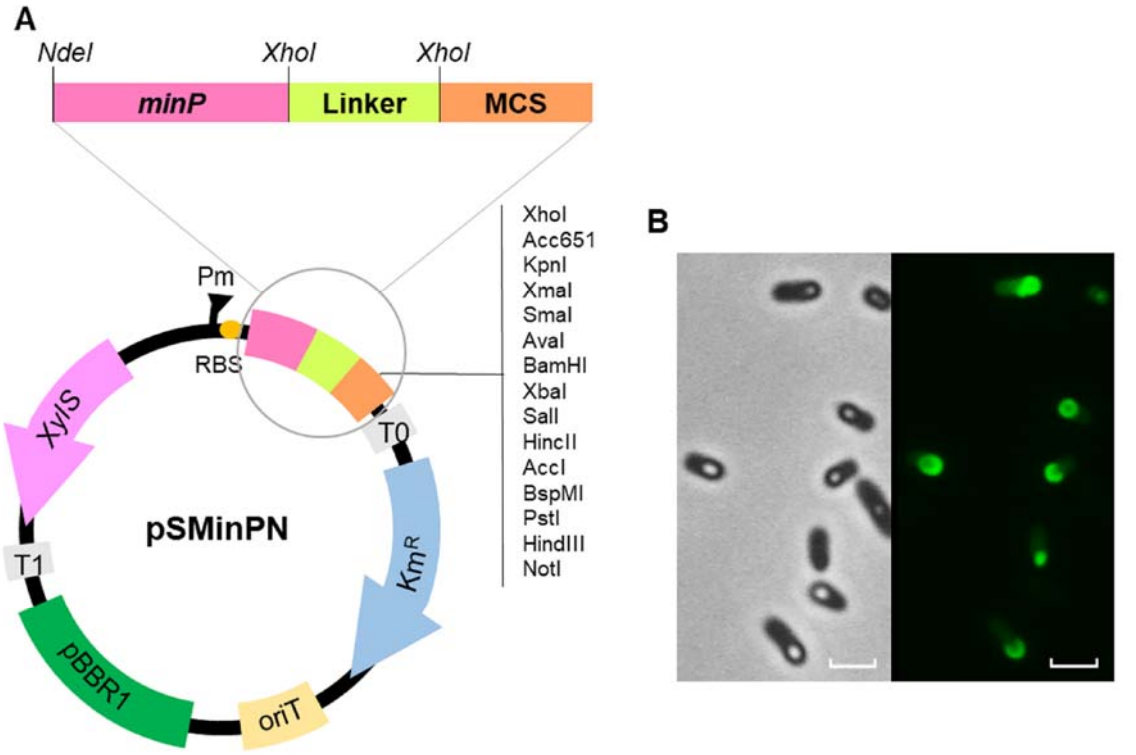

C

>*minP-Linker-MCS*

CATATGGCTGGCAAGAAGAACACCGAAAAAGAAGGCAGCTCCTGGG
TCGGCGGGATCGAGAAATACTCCCGCAAGATCTGGCTGGCGGGGCT
GGGTATCTATTCGAAGATCGACCAGGACGGCCCGAAGCTGTTCGAC
TCGCTGGTGAAGCTCGAGGCAGAAGCGGCAGCCAAAGAGGCGGC
GGCAAAGGAGGCAGCCGCAAAAGAAGCAGCAGCGAAGGAAGCGG
CTGCGAAAGCCGCAGGCTCGGGTGGGTCGGGTGGCTCCGGCGGA
CTCGAGGGTACCCGGGGATCCTCTAGAGTCGACCTGCAGAAGCTT

785

786 **Fig 7.** A) pSMinPN plasmid derived from pSEVA238 to generate MinP N-terminal fusion
787 proteins for the production of customized protein functionalized PHA nanobeads. B) *In vivo*
788 localization of the MinP-GFP produced by *P. putida* KT2440 *Δpha+C1* (pSMinP-1) after 24 h

of growth in PHA producing conditions. Scale bars mean 2 µm. C) Nucleotide sequence of the *minP-Linker-MCS* construction. *minP* gene is represented in pink, Linker region in light green and restriction sites are underlined with different colours (*Nde*I, *Xho*I, *Kpn*I, *BamH*I, *Pst*I, *Xho*I, *Hind*III).

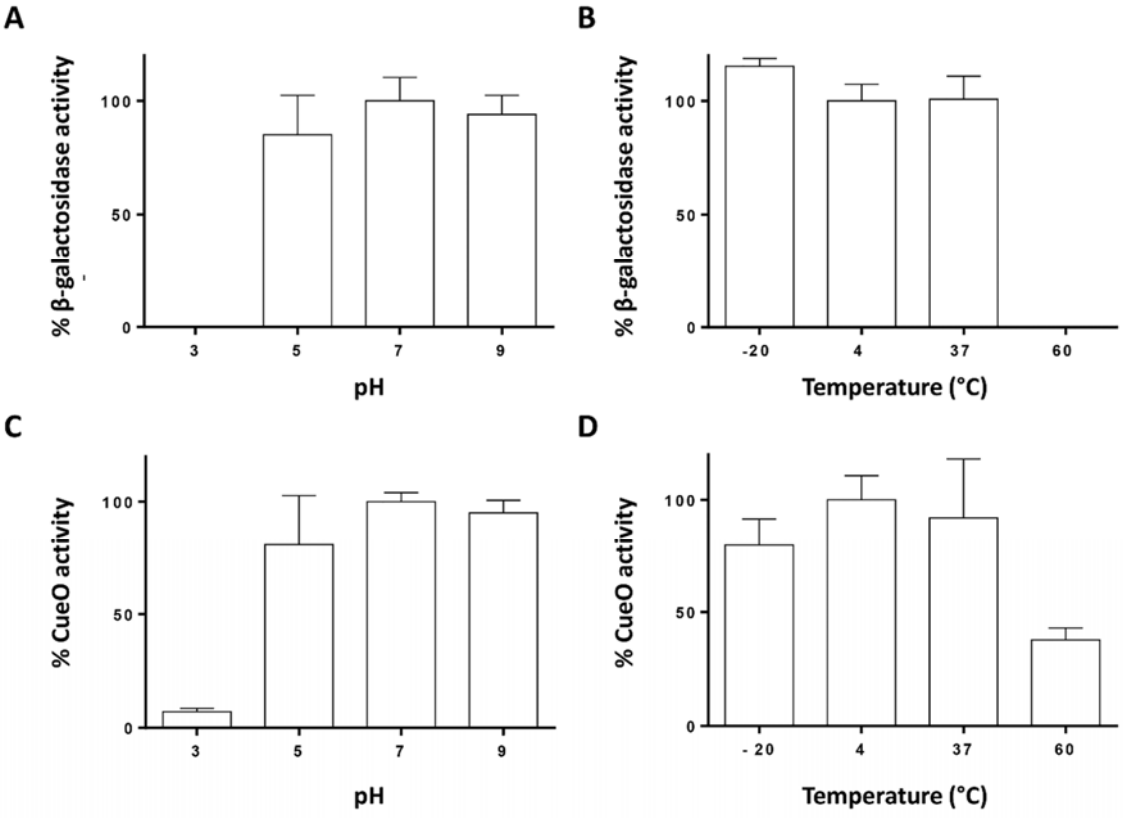

Fig 8. Percentage of activity retained by the protein immobilized at the granule after treatment at different pHs, with respect to a control at pH 7.0 (left panels), or temperatures, with respect to a control at 4 °C (right panels), for both MinP-β-galactosidase (A, B) and MinP-CueO (C, D). Error bars represent SD from 3–5 biological replicates.

799

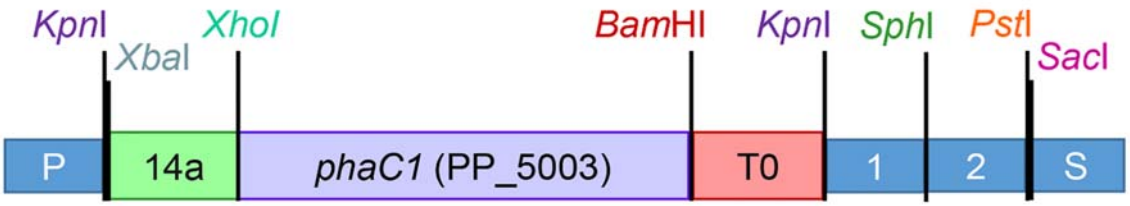

800

801 **Fig 9. *Pha* minimal cluster for the construction of *P. putida* KT2440 Δ*pha*+C1**. 14a:
802 Promoter (49); T0: Lambda T0 terminator. *phaC1:* PhaC1 synthase coding gene from *P.*
803 *putida* KT2440. *P, S, 1* and *2*: overlap regions for Gibson Assembly technique (53).

804

805 **Table 1**. Quantification of PHA production by GC-MS and determination of PHA granule
806 associated protein.

Strain	**CDW (g/L)**	**PHA (% of CDW)**	**Protein on granule surface (mg/g PHA)**	**Protein on granule surface (µM/g PHA)**
KT2440 (WT)	1.47 ± 0.04	70 ± 4	-	-
KT2440 pSP1	0.79 ± 0.00	51 ± 2	-	-
KT2440 pSP1BioF-G	0.90 ± 0.03	54.7 ± 0.6	6 ± 1	0.14 ± 0.03
KT2440 pSP1Bi1-G	0.98 ± 0.05	54.7 ± 2.4	7.4 ± 1.3	0.2 ± 0.04
KT2440 pSP1Bi2-G	0.82 ± 0.01	55 ± 2		
Δpha+C1	0.73 ± 0.04	23 ± 2	-	-
Δpha+C1 pSP1	0.63 ± 0.00	28 ± 4	-	-
Δpha+C1 pSP1BioF-G	0.74 ± 0.05	38 ± 3	8.0 ± 0.7	0.17 ± 0.01
Δpha+C1 pSP1Bi1-G	0.65 ± 0.01	27 ± 4	5.8 ± 0.9	0.16 ± 0.02
Δpha+C1 pSP1Bi2-G	0.59 ± 0.01	27 ± 3	-	-

807

808

809 **Table 2**. Percentage of granule-attached protein after 2 h of the corresponding treatment.

		MinP-CueO	MinP-β-galactosidase
		Mean (%)	**Mean (%)**
pH	3	97 (± 2)	94 (± 10)
	5	96 (± 3)	94 (± 10)
	7	94 (± 5)	97 (± 1)
	9	83 (± 13)	89 (± 8)
[NaCl] mM	0	86 (± 8)	89 (± 3)
	10	96 (± 2)	91 (± 2)
	100	87 (± 8)	98 (± 1)
	1000	91 (± 8)	96 (± 6)
Temperature (°C)	- 20	92 (± 7)	85 (± 9)
	4	96 (± 4)	84 (± 9)
	37	91 (± 5)	76 (± 3)
	60	91 (± 5)	ND

810

811

812 **Table3**. Strains, plasmids and oligonucleotides used in this work.

Strains	**Description**	**Reference**
Pseudomonas putida		
KT2440	Wild-type strain derived of *P. putida* mt-2 cured of the pWW0 plasmid	(45)
KT2440 *Δpha*	Strain with the *pha* cluster deleted	CECT 30020
KT2440 *Δpha+C1*	Strain with *phaC1* genes integrated into the genome of KT2440 *Δpha* under the control of P_{14a} promoter	This work
Escherichia coli		
DH10B	Host for *E. coli* plasmids	Invitrogen, Thermo Fisher Scientific, USA
HB101	Host for plasmid pRK600	(46)
CC118λpir	Host strain for plasmid pTnS-1	(47)
DH5αλpir	Km^R, XylS/*Pm*, pBBR1 ori	Prieto lab collection

Plasmids

pSEVA238	Km^R, XylS/*Pm*, pBBR1 ori	(35)
pSEVA225	Km^R, LacZ, RK2 ori (source of β-galactosidase)	(35)
pCueO	pASK-IBA3 derivative containing the *cueO* sequence. Cm^R, f1 ori	(48)
pSP1	pSEVA238 derivate containing an RBS cloned into *Xba*I and *Hind*III sites	This work
pSP1Bi1-G	pSP1 derivate harboring the fusion gene *bi1-gfp*	This work
pSP1Bi2-G	pSP1 derivate harboring the fusion gene *bi2-gfp*	This work
pSP1Bi3-G	pSP1 derivate harboring the fusion gene *bi3-gfp*	This work
pSP1BioF-G	pSP1 derivative harboring the fusion gene *bioF-gfp*	This work
pSP1Bi4-G	pSP1 derivate harboring the fusion gene *bi4-gfp*	This work

pSMinPN	pSP1 derivate containing the *minP* sequence followed by a glycine rich region and a MCS	This work
pSMinP-1	pSMinPN derivative containing the GFP sequence cloned into *Xho*I and *Hind*III sites	This work
pSMinP-2	pSMinPN derivative containing the *lacZ* sequence cloned into *Xho*I and *BamH*I sites	This work
pSMinP-3	pSMinPN derivative containing the *cueO* sequence cloned into *Xho*I and *Hind*III sites	This work
pTn7	Km^R Gm^R, ori R6K, Tn7L and Tn7R extremes, standard multiple cloning site	(49)
pTn7-ModC1	pTn7 derivate harboring *phaC1* gene	This work
pMAB20-GFP-LYTAG	pMAB20 derivate harboring the fusion gene *bioF-gfp-lytag*	(50)
pRK600	Cm^R, *ori ColE1*, *tra+mob+ of RK2*	(51)
pTnS-1	Ap^R, *ori R6K*, *TnSABC+D* operon	(52)

Oligonucleotide

primers

GFP-F	GGAAGTCCATATGGAACCGCTCGAGATGATCATGGGAATTCAT AA
GFP-R	CATGCAAAGCTTTATTTGTAGAGTTCATCCATGCCG
Bio1-F	GGAAGTCCATATGGCTGGCAAGAAGAACAC
Bio1-R	ATGCACTCGAGCTTCACCAGCGAGTCGAACA
Bio3-F	GGAAGTCCATATGCTTAACAGCGCCATCTCG
Bio3-R	ATGCACTCGAGGCGCGACGAAATCGGCGTAA
Bio4R	ATGCACTCGAGAGTGGTCGAAGACTTGGCAGT
MinPNt-F	GGAAGTCTGAATTCAATAATTTTGTTTAACTTTAAGAAGGAGA TATACATATGGCTGGCAAGAAGAAC
MinPNt-R	ATATCAAGCTTCTGCAGGTCGACTCT
BamHI-GFP-F	GGAAGTCTGGATCCATGCGTAAAGGAGAAGAACT
XhoI-GFP-R	ATATCCTCGAGTGGTACCGGCCACCCCCT
XhoI-CueO-F	AGTCTTCTCGAGGCAGAACGCCCAACGTTACCGAT
HindIII-CueO-R	TCAGAATTCGAAAATATGGCATTTGGGATTG

XhoI-LacZ-F	TCTGGCTCGAGATGACCATGATTACGGATTCACTG
BamHI-LacZ-R	AGTCTTGGATCCATTATTTTTGACACCAGACCAACTG

813